[29] M. Hartig, L. F. Chi, X. D. Liu, H. Fuchs, *Thin Solid Films* **1998**, *327*, 262.
[30] G. Schmid, Y. Liu, *Nano Lett.* **2001**, *1*, 405.
[31] V. Torma, T. Reuter, O. Vidoni, M. Schumann, C. Radehaus, G. Schmid, *ChemPhysChem* **2001**, *8*, 546.
[32] G. Schmid, L. F. Chi, *Adv. Mater.* **1998**, *10*, 515.
[33] Y. Liu, M. Schumann, T. Raschke, C. Radehaus, G. Schmid, *Nano Lett.* **2001**, *8*, 405.
[34] D. Wyrwa, N. Beyer, G. Schmid, *Nano Lett.* **2002**, *2*, 419.
[35] S. Hoeppener, L. Chi, H. Fuchs, *Nano Lett.* **2002**, *2*, 459.
[36] J. Aizenberg, A. J. Black, G. M. Whitesides, *Nature* **1999**, *398*, 495.

Highly Dispersive Micropatterns in Ion-Exchanged Glass Formed by Ion Irradiation Through a Mask of Colloidal Particles**

By *Christof Strohhöfer*, *Jacob P. Hoogenboom*, *Alfons van Blaaderen*, and *Albert Polman**

The optical properties of metallic nanostructures carry considerable interest both from a fundamental and an applications-oriented point of view. The negative values of the real part of the dielectric constant of certain metals, for example, allow the construction of metallodielectric photonic crystals with high dielectric contrast.[1,2] Enhanced transmission of light through apertures with dimensions smaller than the wavelength have led to an ongoing debate about its mechanism.[3,4] Nanometer-sized Ag/Ag_2O nanoclusters on glass have been shown to hold potential for optical data storage.[5]

The focus of this work is the optical constants of composite materials formed by metal nanocrystals in an insulating background material. They are the cause of various interesting optical properties of such materials both in the linear[6] and nonlinear regime.[7] As regards the optical properties, mainly the surface plasmon resonance absorption of such composites has been studied.[8–10] Paired with this absorption is a considerable variation of the real part of the index of refraction.[11,12] Silver nanocrystals in oxide glass have their plasmon resonance absorption in the violet region around 420 nm. The corresponding variation in the real part of the index of refraction of such composites extends from the ultraviolet to the green.

The index of refraction of a glass containing silver ions can thus be changed by nucleating silver nanocrystals. In contrast to many other ions, silver can be introduced into oxide glasses containing network modifiers such as Na^+ or K^+ a posteriori via ion exchange, which allows for the incorporation of silver ion concentrations of several atomic percent. Silver nanocrystals can be formed by ion irradiation of the ion-exchanged glass.[13–15] This formation process, in contrast to annealing in a controlled atmosphere, opens the possibility to nucleate silver nanocrystals in selected regions of a sample only, and thereby changes the index of refraction. A regular pattern of index variations can find application as a diffraction grating, waveguide multiplexer, or photonic crystal. In this article we have explored the formation of such regular refractive index variations, making use of colloidal silica particles deposited on the ion-exchanged glass as an implantation mask. Colloidal particles self-organize on a flat substrate when the solvent evaporates,[16] forming a hexagonal array. Only in the spaces between the particles does formation of silver nanocrystals occur when the sample is irradiated with an ion beam. The outcome is a highly dispersive hexagonal pattern written directly into the glass substrate.

The index of refraction of an unpatterned composite layer was estimated by reflection and transmission measurement according to the method described before.[12] The samples used for this purpose were prepared under identical conditions, but had been ion-irradiated without mask. Figure 1 shows the index of refraction of the planar ion-exchanged and ion-implanted layer estimated from reflection and transmission measurements. The measurements are compared to the index of refraction of the unirradiated glass. The strong features in both the real and imaginary parts of the index of refraction with peaks at 442 nm and 430 nm, respectively, are caused by the surface plasmon resonance of silver nanocrystals in glass.[6] The diameter of the silver nanocrystals is 2 nm

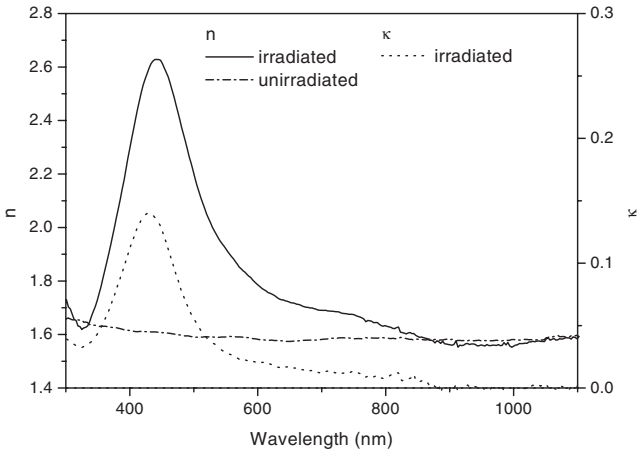

Fig. 1. Real and imaginary parts of the index of refraction of Ag ion-exchanged borosilicate glass before and after ion irradiation. The imaginary part of the glass index of refraction before irradiation does not exceed 2×10^{-5} over the spectral range plotted and is not visible on the scale of the graph. The peaks in both real and imaginary part of the index of the glass after irradiation are caused by the surface plasmon resonance of small silver particles formed in the irradiated layers. The data was obtained from reflection and transmission measurements of samples prepared without a colloidal mask.

[*] Prof. A. Polman, Dr. C. Strohhöfer
FOM Institute for Atomic and Molecular Physics
Kruislaan 407, NL-1098 SJ Amsterdam (The Netherlands)
E-mail: polman@amolf.nl
Dr. J. P. Hoogenboom, Prof. A. van Blaaderen
FOM Institute for Atomic and Molecular Physics
Kruislaan 407, NL-1098 SJ Amsterdam (The Netherlands) and
Debye Institute, Utrecht University
Princetonplein 5, NL-3584 CC Utrecht (The Netherlands)

[**] The authors gratefully acknowledge the help of Hans Zeijlemaker and Ad de Snaijer with the light scattering experiments. They also appreciate the support of Teun van Dillen in the early stages of the experiments. This work is part of the research program of the Dutch Foundation for Fundamental Research on Matter (FOM), and was financially supported by the Netherlands Organisation for Scientific Research (NWO), and the ESPRIT program of the European Union.

  0935-9648/02/2412-1815 $ 17.50+.50/0

ADVANCED MATERIALS

(estimated from a fit of Mie theory[17] to the absorbance of the irradiated layer), with interparticle distances of the order of 10 nm. Both these values are much smaller than the openings in the colloidal mask and than the wavelength of visible light. The glass/Ag nanocrystal composite in the irradiated regions of the masked sample is therefore as homogeneous as the one in the reference sample. This means that the optical constants of the irradiated regions of the masked sample are comparable to the ones determined for the reference sample.

Figure 2 shows a laser scanning microscrope image of the irradiated sample after removal of the colloidal mask. The image was taken in reflection mode at a wavelength of

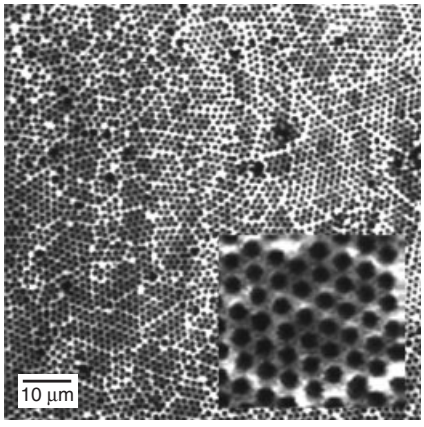

Fig. 2. Reflection image of a region of the sample ion-irradiated through a colloidal mask taken with a laser scanning confocal microscope at a wavelength of 488 nm, after the colloidal particles were removed. Light regions correspond to areas that reflect the light more strongly than dark regions. A hexagonal pattern of circular regions of low reflectivity is seen. This pattern is attributed to the masking effect of a hexagonal array of colloidal spheres with 1.66 μm diameter during ion irradiation. The inset shows a magnified image of a hexagonally ordered domain.

488 nm. The light regions in the image correspond to areas that reflect light more strongly than the dark regions. The image consists of dark circular regions forming a polycrystalline hexagonal pattern in a light background. It is evident that this image reproduced the "shadow" of the colloidal mask, with the dark circles marking the positions held by the silica particles during the ion irradiation. The high reflectivity of the area where the glass/Ag nanocrystal composite has formed (R = 0.16) is a signature of the elevated index of refraction of these regions compared to the base glass (R = 0.05, see Fig. 1). The period of the hexagonal array measured in crystalline domains is 1.68 ± 0.02 μm, in close correspondence to the diameter of the silica particles used as the mask.

Light-scattering experiments were performed to further study the structure of the sample. In this type of experiments, the reciprocal lattice of the scattering array is observed directly. A hexagonal array of scatterers also has hexagonal symmetry in reciprocal space. In Figure 3 we show an image of the scattering pattern in transmission using 442 nm radiation on the same sample as depicted in Figure 2. The polycrystalline configuration leads to the appearance of diffraction rings. Two rings, a strong inner and a weak outer ring (the latter is not shown in Fig. 3), can be discerned. With the modulus of the scattering vector k_{sc} evaluated as

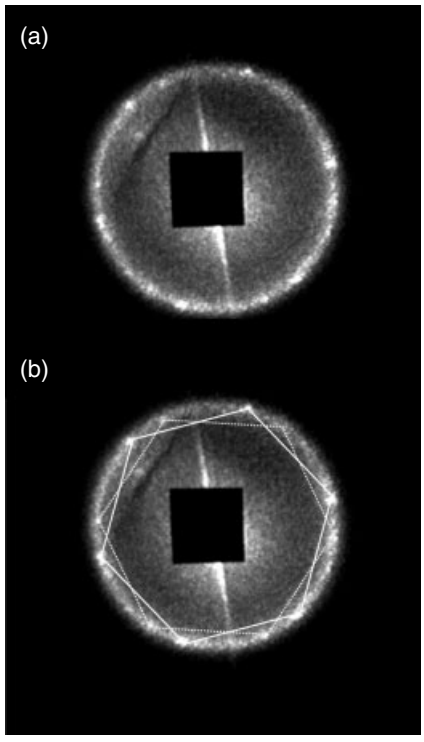

Fig. 3. a) Diffraction image of an ion-exchanged borosilicate glass irradiated through a mask of colloidal spheres. On top of a diffuse ring, bright spots are observed that indicate the hexagonal symmetry of the arrangement of the scatterers. Part (b) shows the same data, overlayed by two hexagons, corresponding to diffraction from two differently oriented domains. The scattering vectors associated with this pattern have a length of around 3.9×10^6 m^{-1}, which corresponds to a lattice constant of 1.6 μm.

$$k_{sc} = \frac{4\pi}{\lambda} \sin\frac{\theta}{2} \quad (1)$$

with λ the wavelength in vacuum of the scattered light and θ the scattering angle, the radii of the two rings correspond to scattering vectors of lengths $(3.9 \pm 0.2) \times 10^6$ m^{-1} and $(7.0 \pm 0.3) \times 10^6$ m^{-1}. The ratio of these two values is $1/\sqrt{3}$ within our measurement error, which is to be expected for hexagonal symmetry. The values correspond to a lattice constant of 1.6 ± 0.1 μm. Identical values for the scattering vectors are obtained when light of different wavelengths in the blue and green is used. The scattering efficiency decreases, however, for longer wavelengths, in correspondence with the decrease of the index contrast (see Fig. 1) and the strong wavelength dependence ($\sim 1/\lambda^4$) of scattering in general. For 633 nm light, the scattered intensity was below the sensitivity of our measurement. Note that Equation 1 describes scattering in vacuum and not in glass. It is valid in our case, however, as the ratio between glass thickness and observation distance is small.

At several places on the sample, the extent of the hexagonal domains is of the order of the footprint of the laser. There the light is scattered mainly from only one or two domains. The bright diffraction spots on the diffuse ring in Figure 3 corre-

  0935-9648/02/2412-1816 $ 17.50+.50/0 *Adv. Mater.* **2002**, *14*, No. 24, December 17

spond to diffraction from such an area. These spots lie on the corners of hexagons, as is seen more clearly in Figure 3b. It shows the same data as Figure 3a, now overlaid with two hexagons connecting two sets of diffraction spots. This correlation is further evidence that diffraction takes place from hexagonally ordered scatterers.

From the width of the diffraction ring we can estimate the average size of the crystalline domains. At small angles (the ring in Fig. 3 corresponds to a scattering angle of 17°), the ratio between width and radius of the diffraction ring is approximately equal to the ratio between lattice constant and average domain diameter. This relation yields an average domain size of 17 μm. This value is in good agreement with the average domain size observed in Figure 2.

Measurements with an atomic force microscope in contact mode reveal that the irradiation with Xe ions changes the morphology of the surface: irradiated regions are elevated by 30 – 40 nm above the unirradiated areas. However, considering the aforementioned wavelength dependence of the scattering efficiency, this physical grating superposed on the index grating is not the principal mechanism causing the diffraction we observe. The wavelength dependence of the scattering efficiency of such a physical grating is considerably weaker than the one observed. Moreover, the scattering volume of the elevated structures is much less than that of the structures in the index grating.

In the present experiment, the size of the colloidal particles used as the irradiation mask has been chosen such that the structures fabricated in the glass are clearly visible in an optical microscope. However, the technique described here is not limited to this size range. Smaller colloidal silica particles are even easier to fabricate than large ones, and self-organize in the same fashion. The lower limit for the period of the grating is the range of the ions used to form silver nanocrystals in the glass. For the conditions used in our experiments, colloidal particles with a diameter of 600 nm are still sufficient to stop 1 MeV Xe ions whose range is around 450 nm in silica. Two possibilities seem viable to further reduce the period of the structure: a reduction of the ion energy used for the irradiation would alleviate the requirements on mask thickness and also produce shallower gratings; the use of different mask materials with higher stopping power for Xe ions, such as Ag or Au,[18] or of anisotropically shaped particles (which have to be made to stand upright) will also lead to a shorter period, whilst leaving unchanged the properties of the glass/Ag nanocrystal layer. Let us also note that techniques have been developed to fabricate two-dimensional single-crystalline arrays of colloidal particles on the centimeter scale. Using such domains of a size greater than the dimensions of the incoming light beam allows the diffracted intensity to be localised in the diffraction spots rather than a diffraction ring. Finally, colloidal particles can be deposited in arrays of symmetries other than hexagonal with the help of optical tweezers or a templated substrate.[19] In this way a variety of diffraction symmetries become available.

In summary, we have fabricated hexagonally ordered arrays of scatterers in ion-exchanged glass by ion irradiation through a hexagonal mask of self-organized colloidal silica particles. The contrast of the refractive index between ion-irradiated and unirradiated regions is caused by the formation of silver nanocrystals under the influence of the ion beam. In light-scattering experiments we observed diffraction patterns corresponding to hexagonal symmetry with a period of 1.6 μm, which correlates well with the diameter of the silica particles used as implantation mask.

Experimental

Borosilicate glass was ion-exchanged for 5 min at 320 °C in a 8.3 mol-% $AgNO_3$/91.7 mol-% $NaNO_3$ melt. Such an ion exchange gives rise to a surface layer in the glass with a graded Ag^+ concentration up to a depth of around 1 μm. The silver concentration at the surface amounts to 7.5 at.-%, as determined by Rutherford backscattering spectrometry. Colloidal silica particles of 1.66 μm diameter were prepared from seeds grown by the usual ammonia-catalyzed Stöber synthesis [20] using a continuous growth set-up as described by Giesche [21]. They were dissolved in ethanol and deposited onto the ion-exchanged glass. The silica particles ordered into a two-dimensional hexagonal array during the evaporation of the solvent [16]. They served as a mask for ion irradiation of the ion-exchanged glass.

The glass with its mask of colloidal particles was cooled to 77 K and irradiated with Xe ions at an energy of 1 MeV to a fluence of 5×10^{15} cm^{-2}. The projected range of the Xe ions in silica is around 450 nm, considerably less than the diameter of the mask particles. During irradiation with heavy ions, silver nanocrystals are formed in the glass [14] in a layer determined by the range of the implanted ions. This layer of glass/silver nanocrystal composite has an elevated index of refraction in the blue and green region of the visible spectrum [12]. After irradiation, the colloidal particles were removed from the surface of the glass.

The samples were analyzed in a confocal laser scanning microscope in reflection mode at a wavelength of 488 nm after removal of the colloidal mask. We used a 100× objective lens with a numerical aperture of 1.4. Light scattering experiments were performed with a He–Cd laser operating at 442 nm in transmission geometry. The footprint of the laser on the sample was around 300 μm. The light scattered by the sample was projected onto a screen and imaged using a CCD camera.

Received: January 7, 2001
Final version: August 12, 2002

[1] A. Moroz, *Phys. Rev. Lett*. **1999**, *83*, 5274.
[2] M. Bockstaller, R. Kolb, E. L. Thomas, *Adv. Mater*. **2001**, *13*, 1783.
[3] T. W. Ebbesen, H. J. Lezec, H. F. Ghaemi, T. Thio, P. A. Wolff, *Nature* **1998**, *391*, 667.
[4] Q. Cao, P. Lalanne, *Phys. Rev. Lett*. **2002**, *88*, 057403-1.
[5] L. A. Peyser, A. E. Vinson, A. P. Bartko, R. M. Dickson, *Science* **2001**, *291*, 103.
[6] U. Kreibig, *J. Phys. F: Met. Phys.* **1974**, *4*, 999.
[7] C. Flytzanis, F. Hache, M. C. Klein, D. Ricard, P. Roussignol, *Progress in Optics XXIX* (Ed: E. Wolf), Elsevier Science, Amsterdam **1991.**
[8] A. Kawabata, R. Kubo, *J. Phys. Soc. Jpn*. **1966**, *21*, 1765.
[9] J. Tiggesbäumker, L. Köller, K.-H. Meiwes-Broer, A. Liebsch, *Phys. Rev. A* **1992**, *48*, R1749.
[10] H. Hövel, S. Fritz, A. Hilger, U. Kreibig, M. Vollmer, *Phys. Rev. B* **1993**, *48*, 18 178.
[11] U. Kreibig, *Z. Phys.* **1970**, *234*, 307.
[12] C. Strohhöfer, A. Polman, unpublished.
[13] G. W. Arnold, J. A. Borders, *J. Appl. Phys.* **1977**, *48*, 1488.
[14] D. P. Peters, C. Strohhöfer, M. L. Brongersma, J. van der Elsken, A. Polman, *Nucl. Instrum. Methods Phys. Res., Sect. B* **2000**, *168*, 237.
[15] E. Valentin, H. Bernas, C. Ricolleau, F. Creuzet, *Phys. Rev. Lett*. **2001**, *86*, 99.
[16] N. D. Denkov, O. D. Velev, P. A. Kralchevsky, I. B. Ivanov, H. Yoshimura, K. Nagayama, *Langmuir* **1992**, *8*, 3183.
[17] G. Mie, *Ann. Phys.* **1908**, *4*, 377.
[18] C. Graf, A. van Blaaderen, *Langmuir* **2002**, *18*, 524.

  0935-9648/02/2412-1817 $ 17.50+.50/0

ADVANCED MATERIALS

[19] A. van Blaaderen, K. P. Velikov, J. P. Hoogenboom, D. L. J. Vossen, A. Yethiraj, R. Dullens, T. van Dillen, A. Polman, in *Photonic Crystals and Light Localization in the 21st Century* (Ed: C. M. Soukoulis), Kluver Academic, Dordrecht, The Netherlands **2001**.
[20] W. Stöber, A. Fink, E. Bohn, *J. Colloid Interface Sci.* **1968**, *26*, 62.
[21] H. Giesche, *J. Eur. Ceram. Soc.* **1994**, *14*, 205.

Modification of Electronic Structures of a Carbon Nanotube by Hydrogen Functionalization**

By *Keun Soo Kim*, *Dong Jae Bae*, *Jae Ryong Kim*, *Kyung Ah Park*, *Seong Chu Lim*, *Ju-Jin Kim*, *Won Bong Choi*, *Chong Yun Park*, and *Young Hee Lee**

The conventional synthesis approaches provide carbon nanotubes (CNTs) with mixed chiralities,[1,2] which are not separable with current technology. This has often been a bottleneck in the application of CNTs to electronic devices such as nanotransistors and memories that require ready-made semiconducting CNTs.[3–5] One alternative approach is to transform the electronic structure of the CNT to that of a large bandgap semiconductor by a post-process treatment. Functionalization of a CNT wall sometimes leads to serious modification of the electronic structure. For instance, fluorination of the CNT modifies the electronic structures to be either metallic or semiconducting, depending on the coverage and method of fluorine application.[6–8] This approach induces a large strain on the tube wall and sometimes deteriorates the CNT. Although metallic multiwalled CNTs could be transformed to semiconducting ones by an effective peeling, this is not easily accessible from technical point of view.[9] A more reliable way to transform metallic CNTs to semiconducting ones with a minimal alteration on the CNT-wall stability is highly desirable.

Here we present a method for CNT functionalization by exposing CNTs to hydrogen atoms. To demonstrate the effect of hydrogen functionalization, we fabricated a CNT–metal junction on a silicon substrate by electron-beam lithography, where one half of each CNT was buried in an SiO_2 layer of 100 nm thickness, and the other half was exposed to air, as shown in Figure 1a. The details have been published before.[10] The exposed part of the CNTs was functionalized by atomic hydrogen, and the half of the CNTs buried in SiO_2 remained unaffected. We should emphasize that this approach to the hydrogenation process is very simple and straightforward without the need to worry about hydrogen bonds being damaged from ultraviolet irradiation, unlike in the previous report.[11]

We prepared two samples: One was metallic (we call this the MS sample) and another was semiconducting with an energy gap of 0.8 eV (we call this the SS sample). Both samples showed an ohmic behavior at near room temperature (Fig. 1b), with a resistance of 155 kΩ for the pristine MS sample, and 10 MΩ for the pristine SS sample. The *I*–*V* (current–voltage) characteristics were significantly changed after hydrogenation, as shown in Figure 1b. Rectifying effects were observed for both samples. The anisotropy, which can be defined as

$$\alpha = \left| I(V_d = 2V)/I(V_d = -2V) \right| \quad (1)$$

was 5 and 10 for the respective MS and SS samples, i.e., the rectifying effect was more prominent in the SS sample. We emphasize that both samples were operable as a rectifier at room temperature. The differential conductance d*I*/d*V* was finite near the zero-bias region at 5.6 K in the pristine MS sample (inset of Fig. 1c), suggesting this sample to be nearly metallic. The pristine SS sample revealed a vanishing conductance near the gap region (inset of Fig. 1d), suggesting it to be a semiconducting CNT. We estimated the contact-barrier height, ϕ_b, between the metal electrode and the pristine CNT from an Arrhenius plot and an extrapolation to zero-drain voltage by assuming that *I*–*V*–*T* (current–voltage–temperature) characteristics follow the thermionic electron emission model, and θ_b is proportional to the square root of the drain voltage.[12] The contact barriers were determined to be 14 meV and 60 meV for the pristine MS and SS samples, respectively. We also evaluated the energy gap of the semiconducting SS sample. Since two metal–CNT contacts were formed in series, the energy gap can be defined as half of the zero-conductance region confined by the abrupt increase in the conductance at low temperature (inset of Fig. 1d).[13] The energy gap was about 0.8 eV, similar to that obtained in a previous scanning tunneling spectroscopy study.[14] After hydrogenation, a clear energy gap of 1.88 eV was observed in the MS sample, and the conductance increased almost linearly above the gap region, as shown in Figure 1c. The energy gap was modified to 4.4 eV in the hydrogenated SS sample, which is more severely widened compared to that of the hydrogenated MS sample.

The rectifying diode effect is clearer when we look at the gating effect, as shown in Figure 2. No gating effect was observed at low temperature in the pristine MS sample, suggesting that the MS sample is simply a metallic tube. Since the current flow is symmetric with respect to the polarity of the drain voltage, two metal–CNT contacts were formed symmetrically. After hydrogenation, this sample became semiconducting even at room temperature, revealing the gating effect with a hole-type carrier, where the current is suppressed at positive

[*] Prof. Y. H. Lee, K. S. Kim, Dr. D. J. Bae, K. A. Park, Dr. S. C. Lim, Prof. C. Y. Park
Department of Physics and Institute of Basic Science
Center for Nanotubes and Nanostructured Composites
Sungkyunkwan University, Suwon, 440-746 (Korea)
E-mail: leeyoung@yurim.skku.ac.kr
J. R. Kim, Prof. J.-J. Kim
Department of Physics, Chonbuk National University
Chonju 561-756 (Korea)
Dr. W. B. Choi
Memory Device Laboratory, Samsung Advanced Institute of Technology
Suwon 440-600 (Korea)

[**] This project was supported in part by the MOST through National Research Laboratory program and New Frontier project, and in part by the CNNC at SKKU.

  0935-9648/02/2412-1818 $ 17.50+.50/0 *Adv. Mater.* **2002**, *14*, No. 24, December 17